

Dry Transfer Based on PMMA and Thermal Release Tape for Heterogeneous Integration of 2D-TMDC Layers

Amir Ghiami,^{†,} Hleb Fiadziushkin,[†] Tianyishan Sun,[†] Songyao Tang,[†] Yibing Wang,[†] Eva Mayer,[‡] Jochen M. Schneider,[‡] Agata Piacentini,^{§,α} Max C. Lemme,^{§,α} Michael Heuken,^{†,§} Holger Kalisch,[†] Andrei Vescan[†]*

[†] Compound Semiconductor Technology, RWTH Aachen University, 52074 Aachen, Germany

[‡] Materials Chemistry, RWTH Aachen University, 52074 Aachen, Germany

[§] Advanced Microelectronic Center Aachen (AMICA), AMO GmbH, 52074 Aachen, Germany

^α Chair of Electronic Devices, RWTH Aachen University, 52074 Aachen, Germany

[§] AIXTRON SE, 52134 Herzogenrath, Germany

* Corresponding author: ghiami@cst.rwth-aachen.de

KEYWORDS: *2D-TMDC, scalable integration, dry transfer, field-effect transistor*

ABSTRACT: A reliable and scalable transfer of 2D-TMDCs (two-dimensional transition metal dichalcogenides) from the growth substrate to a target substrate with high reproducibility and yield is a crucial step for device integration. In this work, we have introduced a scalable dry-transfer approach for 2D-TMDCs grown by MOCVD (metal-organic chemical vapor deposition) on sapphire. Transfer to a silicon/silicon dioxide (Si/SiO₂) substrate is performed using PMMA (poly(methyl methacrylate)) and TRT (thermal release tape) as sacrificial layer and carrier, respectively. Our proposed method ensures a reproducible peel-off from the growth substrate and better preservation of the 2D-TMDC during PMMA removal in solvent, without compromising its

adhesion to the target substrate. A comprehensive comparison between the dry method introduced in this work and a standard wet transfer based on potassium hydroxide (KOH) solution shows improvement in terms of cleanliness and structural integrity for dry-transferred layer, as evidenced by X-ray photoemission and Raman spectroscopy, respectively. Moreover, fabricated field-effect transistors (FETs) demonstrate improvements in subthreshold slope, maximum drain current and device-to-device variability. The dry-transfer method developed in this work enables large-area integration of 2D-TMDC layers into (opto)electronic components with high reproducibility, while better preserving the as-grown properties of the layers.

1. INTRODUCTION

Two-dimensional transition metal dichalcogenides (2D-TMDCs), recognized for their exceptional electronic, physical and chemical properties, are rapidly emerging on the forefront of research on solid-state micro-/nanoelectronic devices and circuits.¹ It has been suggested that these materials could extend Moore's law and pioneer innovative devices beyond CMOS (complementary metal-oxide-semiconductor) technology.² By 2028, the International Roadmap for Devices and Systems (IRDS) anticipates 2D-TMDC materials to find commercial applications in transistors and beyond-CMOS devices.³

Despite the impressive performance of devices based on 2D-TMDC layers created via mechanical exfoliation from bulk crystals, industrial scaling still presents a significant challenge. Synthesizing high-quality 2D-TMDCs requires elevated growth temperatures of 700-900 °C, which exceed the CMOS back-end-of-line (BEOL) integration limit (< 400 °C).⁴ Additionally, optimized 2D-material growth is mostly performed on substrates different from conventional device templates like silicon/silicon dioxide.⁵⁻⁹ This underscores the importance of developing robust and scalable methods to transfer 2D-TMDC films from their growth substrates onto device

templates. Various methods have been developed to transfer 2D materials, which typically fall into “dry” and “wet” categories.¹⁰⁻¹² Within the community, there has been particular focus on dry methods in the last years, likely due to their scalability and automatability.¹⁰ During the dry transfer of 2D-TMDC materials, a sacrificial layer is essential to provide a mechanical support and maintain the integrity of the 2D layer throughout the transfer process.¹¹ Polymers such as PMMA are commonly used for this purpose and are applied via spin-coating.¹³⁻¹⁷ The mechanical properties of PMMA largely depend on its molecular weight (MW); therefore, high-MW PMMA (e.g. 950 K) is typically used to ensure sufficient mechanical support and prevent damage to the 2D material.^{18,19} In the dry method, to peel-off the 2D-TMDC/PMMA stack from the growth substrate, a TRT (alternatively laser- or UV-release tape) serving as a carrier is attached on top of the spin-coated and baked polymer layer. The 2D-TMDC/polymer/tape stack is then delaminated through a mechanical peel-off.^{12,16,20,21} Subsequently, the peeled stack is positioned onto the target substrate. The carrier tape is then delaminated by reducing its adhesion through heating (or laser/UV exposure).^{12,16,22} Finally, the polymer is removed using chemical solvents.

While the dry-transfer steps may appear straightforward, this method still faces several obstacles, particularly in terms of yield and reproducibility. One issue is the process of peeling-off the 2D-TMDC/polymer stack from the growth substrate, which may result in the 2D-TMDC/polymer layer remaining partially or completely undetached. To address this, some methods incorporate a (semi)metallic interfacial layer (such as gold²³ or bismuth²⁴) between the 2D-TMDC and the polymer. These layers, which adhere strongly to the 2D-TMDC and the polymer, are thought to improve peel-off yield. However, this adaption requires an additional metal etching step using acid at the end of the process, which can lead to further damage or contamination of the 2D-TMDC film.

Another complication arises in the final step during polymer removal with chemical solvents, during which the 2D-TMDC layer might partially or entirely detach from the target substrate which is rooted in a comparably weak adhesion.^{10,20,25} This issue was addressed in a recent work by Kwon *et al.*,²⁰ in which a 2D-MoS₂ layer was successfully dry-transferred onto a prepatterned Si/SiO₂ substrate with Au contacts using PMMA and TRT. The high yield achieved after PMMA removal (in hot acetone) was facilitated by the strong adhesion between the Au surface and 2D-MoS₂. Additionally, they showed that the total thickness of the bottom contact should be maintained below 30 nm to preserve the 2D-MoS₂ during PMMA removal. However, their method is limited to prepatterned substrates only, and dry transfer of 2D-TMDCs on target substrates like Si/SiO₂ still remains a challenge due to the weak adhesion between SiO₂ and 2D-TMDC.

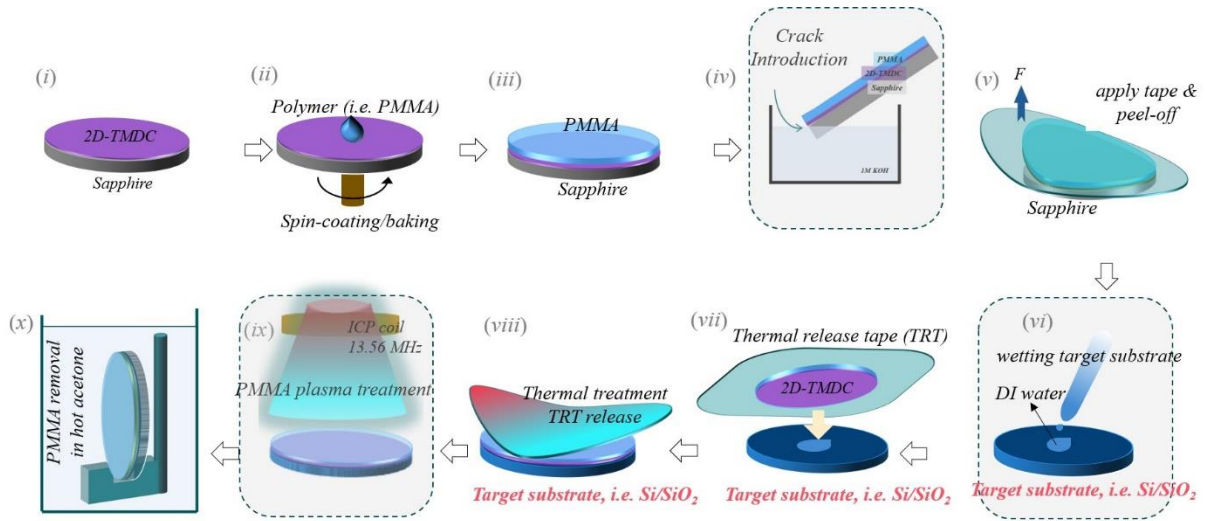


Figure 1. Detailed schematics of the dry transfer steps using PMMA and TRT; the steps developed in this study are outlined (i) as-received 2D-TMDC on growth substrate (*i.e.* sapphire), (ii) PMMA spin-coating and baking, (iii) PMMA spin-coated 2D-TMDC on sapphire, (iv) crack introduction at the edge of the stack between sapphire and 2D-TMDC/PMMA before applying the TRT, (v) TRT application and peel-off, (vi) wetting the target substrate with DI water droplet before transferring the peeled-off 2D-TMDC/PMMA/TRT stack. (vii) transfer the 2D-TMDC/PMMA/TRT stack onto the target substrate, (viii) TRT removal and annealing on hot plate, (ix) inductively coupled plasma (ICP) treatment of the PMMA layer, (x) PMMA removal in hot acetone.

Our work based on the dry-transfer approach using PMMA and TRT aims to tackle the described challenges by: (1) improving the peel-off of 2D-TMDC/polymer from the growth substrate (*i.e.* sapphire) and (2) a better preservation of the 2D-TMDC layer on the target substrate (*i.e.* Si/SiO₂)

during the polymer removal with chemical solvents. The wafer-scale dry transfer process flow proposed in this work is schematically illustrated in Figure 1.

2. RESULTS AND DISCUSSION

2D-WSe₂ deposited on 2" sapphire substrates via a commercial AIXTRON CCS MOCVD (metal-organic chemical vapor deposition) tool was chosen as 2D-TMDC material in this work. For our studies, 3 × 3 cm² samples were cleaved from the wafer centers. Then, the PMMA was spin-coated on top and backed in air.

In the following step, in order to improve the peel-off process (the first aim of our work), we introduce a crack at the perimeter of the stack between growth substrate (sapphire) and the 2D-WSe₂/PMMA layer, using a KOH solution (in analogy with Fig. 1 (iv)). This was performed by 30 s – 60 s exposure to a 1 M KOH solution. The crack serves as the initiation point for the subsequent peel-off. As the KOH solution, unlike in wet-transfer methods,¹⁷ only wets a small section of the 2D film edge, it does not impair the quality of the 2D-TMDC layer.

Next, a piece of TRT was applied onto the sample. Subsequently, a gentle mechanical peel-off was initiated by removing the 2D-WSe₂/PMMA/TRT, starting from the already cracked edge (cf. Fig. 1 (v)). Numerous experiments have demonstrated that such crack introduction at the edge of the stack consistently leads to a successful peel-off of the complete sample area. This is due to the fact that the majority of the force required is for the crack initiation (first stage of peel-off), which involves overcoming the inherent toughness of the material. Once initiated, crack propagation (second stage of peel-off) occurs with considerably less force, according to well-established principles in fracture mechanics.^{21,26}

In the next step, inspired by direct wafer bonding techniques,^{27,28} we wetted the Si/SiO₂ target substrate (with 100 nm thermally grown SiO₂) with DI water droplets before transferring the

peeled-off stack. DI water obviously displaces air and fills the gap between 2D-WSe₂ and the target substrate. It should be noted that, before transferring the stack, the extra tape overhang around the 2D-WSe₂ layer was cut away. The stack was then left for about 6 *h* at ambient temperature in a tilted position to allow the water to slowly diffuse laterally out of the interface, enabling the 2D-WSe₂ to conform to the target substrate and improve bonding.

After 6 *h* rest time, the stack was heated from room temperature to the 90°C tape release temperature on a hot plate to remove the tape. Following tape removal, the stack was further heated to ~150°C and maintained at that temperature for 10 *min* to further enhance the adhesion between 2D-TMDC and the target substrate (as illustrated in Fig. 1 (viii)).

In the following step, PMMA needs to be removed in hot acetone. In previous works, it was observed that performing this step directly causes partial detachment of the 2D-TMDC from the target substrate, particularly within the first minute of immersion. When PMMA is initially exposed to acetone, rapid solvent diffusion and polymer swelling lead to a significant release of mechanical stress in PMMA,^{20,29} which, to our understanding, can disrupt the adhesion of the 2D material to the target substrate. By ensuring a slower, more controlled PMMA removal during this initial stage, this issue is expected to be resolved effectively. Therefore, the PMMA surface was treated with Ar/BCl₃ plasma in an inductively coupled plasma (ICP) chamber (as shown in Fig. 1 (ix)).³⁰ When PMMA is exposed to an inert plasma like Ar, high-energy ions and electrons can induce cross-linking on the polymer surface. This process, known as CASING (cross-linking by activated species of inert gas), involves the formation of covalent bonds between polymer chains, increasing the overall molecular weight of the surface layer.³⁰⁻³² In addition, BCl₃ plasma might further increase the molecular weight by forming a more cross-linked polymer. As intended, such

a densified surface layer acts as a controlled barrier slowing down acetone penetration and successfully preventing TMDC detachment.

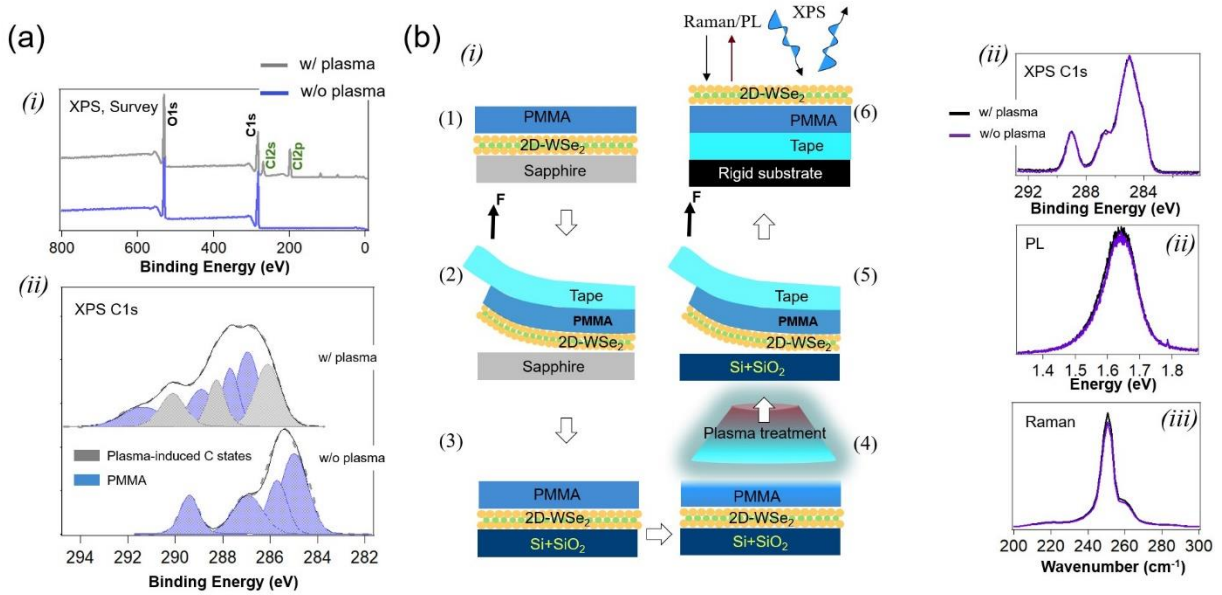


Figure 2. (a) Chemical analyses of plasma treated PMMA surface, (i) XPS survey scans, (ii) high resolution XPS C1s core level. (b) Exploring the potential impact of plasma treatment on the underlying 2D-WSe₂ and 2D-WSe₂/PMMA interface: (i) process steps to prepare 2D/PMMA/tape stack to access 2D and 2D/PMMA interface avoiding thick PMMA film, (ii) comparison of the XPS, PL and Raman signals of the 2D-WSe₂ and 2D-WSe₂/PMMA interface in plasma-treated and untreated stacks.

To verify our hypothesis of a densified PMMA surface and to exclude other effects of plasma treatment on the PMMA, X-ray photoemission spectroscopy (XPS) was performed. The XPS survey spectra of as-prepared PMMA and plasma-treated PMMA are shown in Figure 2a (i). In the as-prepared PMMA, only carbon and oxygen peaks are visible, while plasma-treated PMMA shows additional peaks attributed to chlorine (Cl), indicating the incorporation of Cl species during plasma exposure. The high-resolution C1s spectra of both PMMA samples are shown in Figure 2a (ii). The as-prepared PMMA reveals characteristic PMMA peaks, highlighted in blue, with four distinct components: (1) hydrocarbon (C–C/C–H) at a binding energy of 285 eV, (2) β -shifted carbon at 285.7 eV, (3) methoxy group carbon at 286.8 eV and (4) carbon in the ester group at 289.1 eV.^{33,34} The plasma-treated PMMA shows two key differences. First, the PMMA-associated peaks are shifted toward higher binding energies, which can be attributed to increased cross-

linking and incorporation of a highly electronegative specie (*i.e.* Cl) caused by plasma-induced modifications.³⁰ Additionally, three new peaks appear, likely due to plasma-induced carbon states associated with bond formations between carbon and Cl or cross-linked carbon structures, consistent with the changes expected from Ar/BCl₃ plasma treatment.^{35–37}

To further confirm that plasma treatment only affects the surface of the PMMA without altering the 2D-TMDC layer or the 2D-TMDC/PMMA interface, we conducted XPS, Raman and photoluminescence (PL) spectroscopy (Fig. 2b). For this purpose, two sets of 2D-WSe₂/PMMA stacks were prepared: one with PMMA plasma treatment and one without. The stack preparation steps are shown in Figure. 2 b (i) and include a second transfer, exposing the 2D-WSe₂ film on top of PMMA (either treated or untreated)/TRT. This approach allows accessing the 2D-WSe₂ and the 2D-WSe₂/PMMA interface directly from the TMDC side. The XPS, PL and Raman spectra of both stacks show negligible differences, suggesting an unaffected 2D-WSe₂ and 2D-WSe₂/PMMA interface after plasma treatment. (Fig. 2b (ii))

Figure 3a illustrates the main transfer steps for a 3 × 3 cm² 2D-WSe₂/sapphire sample. Figure 3a (iv) shows the successfully transferred 2D layer on SiO₂/Si after PMMA removal, with no visible macroscopic defects or pinholes as evaluated by optical microscopy (Fig. 3b (iv)). The improved adhesion of the 2D-TMDC to Si/SiO₂, along with the more controlled PMMA removal—achieved through wetting the target substrate and PMMA plasma treatment—contributed to the preservation of the 2D-TMDC. Without these measures, partial detachment of the 2D-TMDC layer frequently occurs; examples of such failures are presented in Figure 3b (i)-(iii). Figure 3c (i) and (iii) display the Raman and PL maps of the transferred 2D-WSe₂ layer, respectively, along with the corresponding spectra (Fig. 3c (ii) and (iv)). Both the Raman and PL data confirm the uniformity and superior integrity of the transferred layer.

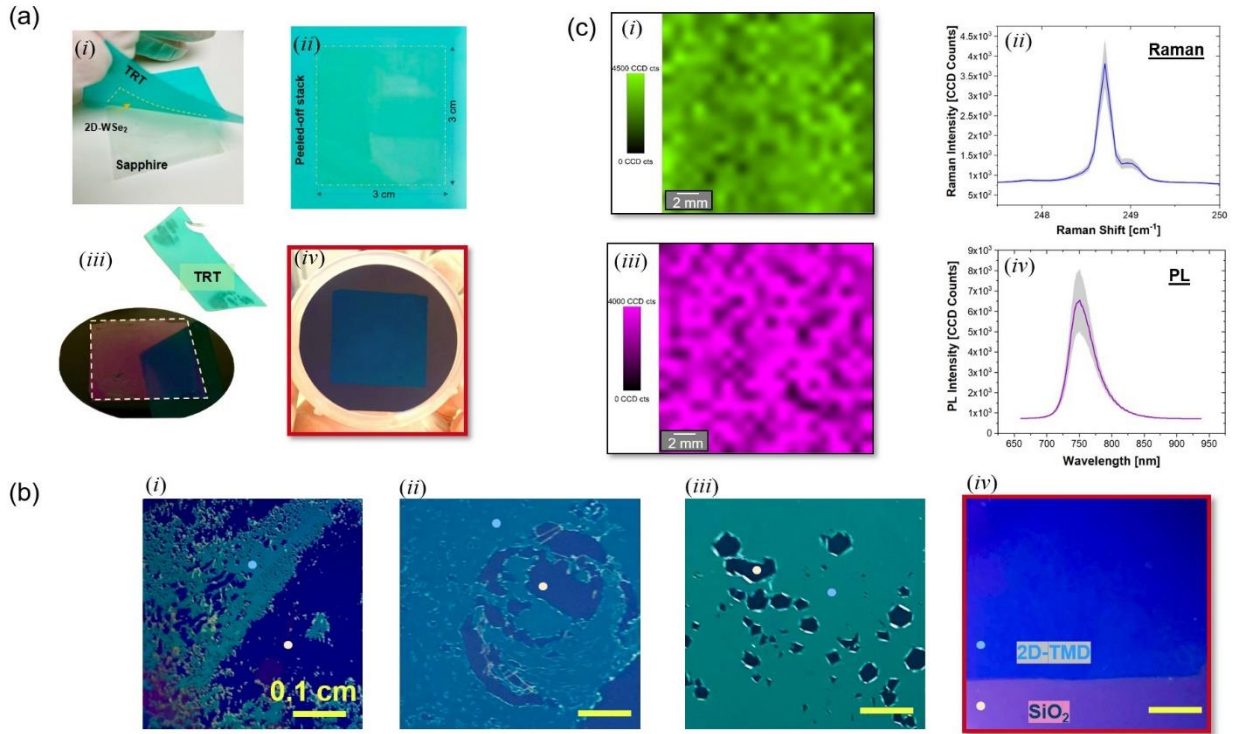


Figure 3. (a) Main dry transfer steps for a $3 \times 3 \text{ cm}^2$ 2D-WSe₂/sapphire sample: (i) peel-off, (ii) peeled 2D-WSe₂/PMMA/TRT stack, (iii) removing the tape and annealing the stack on a hot plate, (iv) 2D-WSe₂ layer on target substrate (Si/SiO₂) after PMMA removal. (b) Impact of target substrate wetting and PMMA plasma treatment on the dry transfer yield: The optical microscope images show the 2D-TMDC after transfer and PMMA removal in hot acetone; (i) without substrate wetting and plasma treatment, (ii) with substrate wetting but no plasma treatment, (iii) with plasma treatment but no substrate wetting; in all three cases, severe 2D-TMDC detachment and pinholes are visible. (iv) with both substrate wetting and plasma treatment, achieving 100% transfer yield with no detachment/pinholes visible under optical microscope (image b (iv) highlights an area near the edge of the transferred layer to better visualize the 2D-TMDC and substrate). In (b), blue and pink spots point on 2D-TMDC and target substrate regions, respectively. (c) Raman and PL characterization of the dry-transferred 2D-WSe₂ layer: (i) Raman map and (ii) corresponding spectrum with raw data in greyscale; (iii) PL map and (iv) corresponding spectrum with raw data in greyscale.

Additionally, to further demonstrate the efficacy of the developed dry transfer method we transferred a 2D-MoS₂ layer onto a prepatterned substrate with 50 nm Au contacts, comparable to Kwon *et al.*²⁰. Even on a structured template, our transferred layer showed near-perfect transfer yield with no defects or pinholes visible under optical microscope after PMMA removal (see Supporting Information).

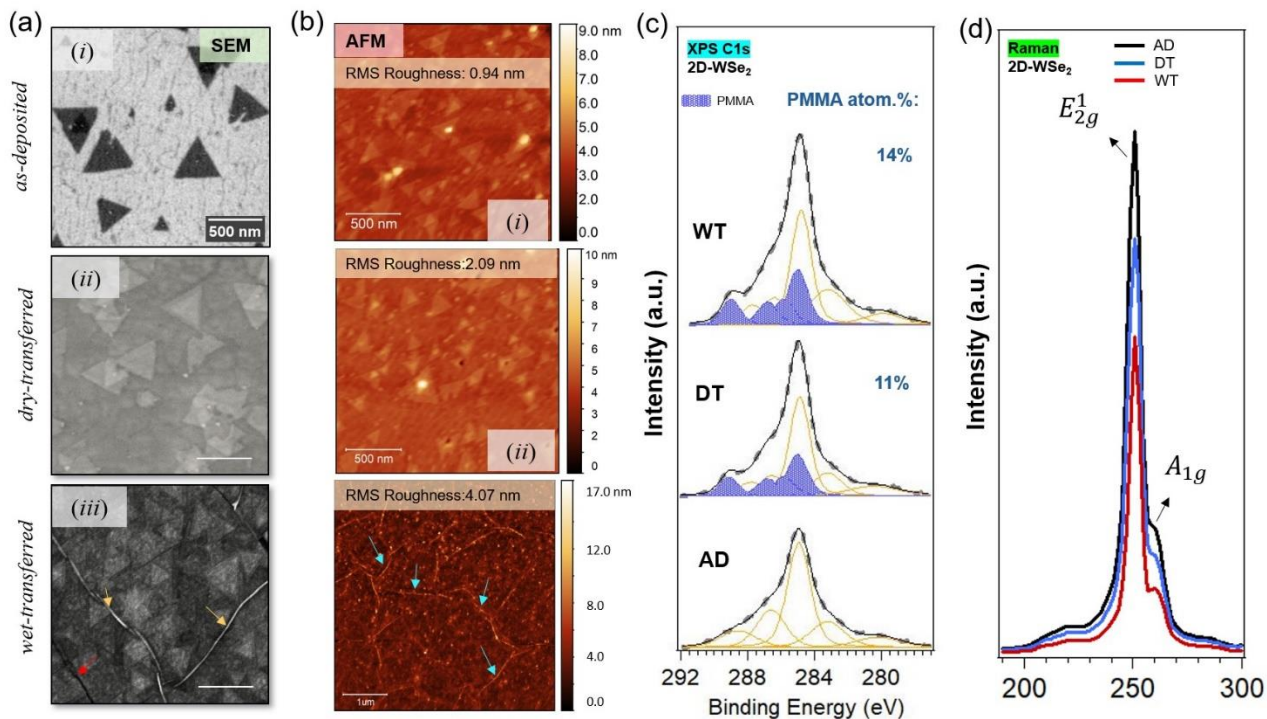


Figure 2. Characterization of the as-deposited and transferred 2D-WSe₂ layers. (a) SEM images of (i) as-deposited, (ii) dry-transferred and (iii) wet-transferred 2D-WSe₂. In the wet transferred sample, wrinkles and cracks are highlighted by yellow and red arrows, respectively. The scale bar size is 500 nm for all images. (b) AFM images of (i) as-deposited, (ii) dry-transferred and (iii) wet-transferred 2D-WSe₂. In the wet transferred layer, the 2D-TMDC nuclei are not visible due to a high density of wrinkles. (c) High resolution XPS *C1s* spectra of as-deposited versus dry- and wet-transferred 2D-WSe₂ (after PMMA removal). (d) Raman spectra of as-deposited versus dry- and wet-transferred 2D-WSe₂. As-deposited, dry-transferred and wet-transferred samples are denoted as AD, DT and WT, respectively.

In order to assess the quality and cleanliness of the 2D-WSe₂ layers dry-transferred onto Si/SiO₂ substrate and to provide a comparison with those after standard KOH-assisted wet transfer (described by Schneider *et al.*³⁸), scanning electron microscopy (SEM), atomic force microscopy (AFM), Raman spectroscopy, and XPS were performed. Figure 4a (i) presents an SEM image of the as-deposited 2D-WSe₂, which is a coalesced monolayer with approx. 30% bilayer coverage. Figure 4a (ii) and (iii) show the dry- and wet-transferred layers after PMMA removal. The dry-transferred layer appears free of wrinkling and cracking. In contrast, the wet-transferred counterpart (Fig. 4a (iii)) exhibits wrinkles and cracks formed during wet transfer (Fig. 4a (iii)).

AFM images of the as-deposited, dry- and wet-transferred layers are presented in Figure 4b (i)-(iii), respectively. A root mean square (rms) roughness of 0.94 nm was measured for the as-

deposited layer. The dry-transferred layer exhibits an increase in rms roughness to about 2 nm, likely due to some PMMA residues remaining on the surface. The wet-transferred layer shows an even higher rms roughness of approximately 4 nm, probably to be attributed to the higher amount of polymer residues and the presence of wrinkles (indicated by blue arrows).

XPS analyses of the as-deposited and transferred layers have been performed. The fitted high-resolution XPS *C1s* core levels of the as-deposited as well as wet- and dry-transferred layers are shown in Figure 4c. The detected carbon signals can be referred to three different sources, (1) co-deposited carbon during MOCVD,³⁹ (2) adventitious carbon and (3) PMMA. The peaks attributed to the first two sources are shown in yellow. The PMMA-associated peaks filled in blue are resolved in four components as described previously. The amount of PMMA residues calculated based on its atomic percentage are also shown in Figure 4c. It was observed that dry-transferred layers contained up to 23% less PMMA relative to wet-transferred ones. Although dry transfer reduces PMMA residues to some extent, a considerable amount still remains, which can adversely affect the performance of devices based on these transferred layers.^{40,41} Addressing this challenge is critical for future improving 2D-TMDC-based devices. More details on the chemical composition of the as-deposited, dry- and wet-transferred 2D-WSe₂ layers are provided in the Supporting Information.

Raman spectra of the as-deposited, dry-transferred, and wet-transferred layers are depicted in Figure 4d. The characteristic WSe₂ Raman peaks, namely E_{2g}^1 and A_{1g} , were observed at 250 cm^{-1} and 261 cm^{-1} , respectively.^{42,43} The spectra revealed a lower intensity for wet-transferred layer in comparison to the dry-transferred counterpart. This reduction in intensity could be due to three factors: (1) PMMA residues may partially absorb or scatter incoming and reflected light; (2)

molecular interactions between PMMA and the underlying 2D film; and (3) a better preservation of layer quality and reduced damage after the dry transfer method.^{25,44}

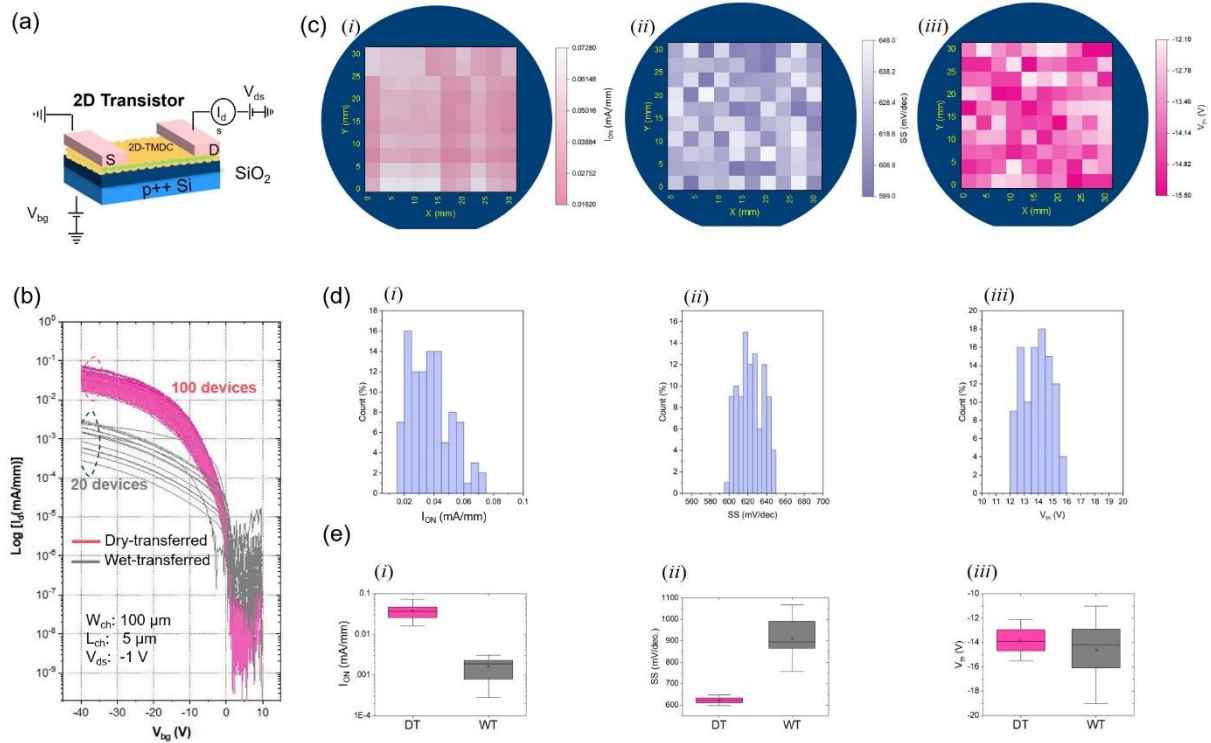


Figure 3. Field-effect transistors based on dry- and wet-transferred 2D-WSe₂ layers: (a) schematic illustration of globally back-gated field-effect transistors used in this study, (b) I - V transfer characteristics of transistors based on dry- and wet-transferred 2D-WSe₂ layers. (c) Spatial map of (i) ON current, (ii) subthreshold slope, and (iii) threshold voltage variations within the 3×3 cm² region of transistors fabricated using dry-transferred layer. (d) Histograms showing the distribution of (i) ON current, (ii) subthreshold swing, and (iii) threshold voltage values of the maps in (c). (e) comparison of the device metrics for transistors based on dry- and wet-transferred layers. Dry-transferred and wet-transferred are denoted as DT and WT, respectively.

To evaluate and compare the electrical performance of 2D-WSe₂ layers obtained via dry and wet transfer, field-effect transistors (FETs) were fabricated. A large 3×3 cm² dry-transferred layer (shown in Fig. 3a (iv)) and a 1×1 cm² wet-transferred layer were used for device fabrication and characterization. Gold (Au) was used as the top contact, with highly p-type doped Si serving as a global back gate with 100 nm thermally-grown SiO₂ layer as the gate dielectric. The devices were measured under ambient condition. The FET layout is schematically illustrated in Figure 5a (channel length (L_{Ch}) of 5 μ m, channel width (W_{Ch}) of 100 μ m).

To assess device metrics, ON currents (I_{ON}) were extracted at a drain bias $V_{DS} = -1$ V, and back-gate voltage $V_{BG} = -40$ V.⁴⁵ Moreover, the subthreshold slope (SS) was determined based on the following equation:^{46,47}

$$SS = \frac{d V_{BG}}{d \log I_D} \quad (1)$$

, where I_D is the drain current. In addition, the threshold voltage (V_{th}) of the devices was extracted using the linear extrapolation method.⁴⁸

In total, 100 FETs across a 3×3 cm² area were measured for the dry-transferred layer, and 20 devices based on wet-transferred layer (1×1 cm²) were evaluated. The I - V transfer characteristics of all devices are shown in Figure 5b. Figure 5c (i)-(iii) displays the spatial variation maps for I_{ON} , SS and V_{th} of the FETs based on dry-transferred 2D-WSe₂. The corresponding distributions are shown in the histograms in Figure 5d (i)-(iii). The variations of device metrics indicate that the device performance is uniform over the 3×3 cm² area.

The comparison of device metrics, namely I_{ON} , SS , and V_{th} , between wet- and dry- transferred layers is summarized in Figure 5e (i)-(iii). The FETs based on dry-transferred layers demonstrate significant improvement in the extracted device parameters, with an over 50× increase in the average I_{ON} compared to wet-transferred counterpart. (Fig. 5e (i)) For the SS , devices based on dry-transferred layers exhibit values approximately 1.5× smaller than those based on wet-transferred layer. Additionally, the threshold voltage for devices based on dry transferred layers shows a significantly narrower distribution.

Device-to-device variability for the device metrics was also quantified using the coefficient of variation (CV), calculated as the ratio of the standard deviation to the mean value ($CV = \frac{\sigma}{\mu}$). The CV for I_{ON} of dry- and wet-transferred was found to be 0.338 and 1.124, respectively. For the SS , the CV values for dry- and wet-transferred were 0.2428 and 0.3053, respectively. As for threshold

voltage, the obtained CV values were found to be 0.4852 and 0.6247, for devices based on dry- and wet- transferred layers, respectively. These results demonstrate that dry-transferred layers provide more consistent performance with lower device-to-device variability. The improvement in electrical performance observed for dry-transferred layers can be attributed to the absence of wrinkles, cracks and KOH-related degradation,¹⁷ and a lower degree of polymer contamination.

3. CONCLUSION

In this work, we have developed a dry transfer method for 2D-TMDC materials utilizing widely available materials, PMMA and thermal release tape. This method effectively addresses the challenges associated with preserving 2D-TMDC layer during PMMA removal, ensuring minimal damage and maintaining layer integrity. Compared to the standard KOH-assisted wet transfer process, the dry method better retains the quality of the as-deposited 2D-TMDC layer, as confirmed by Raman, XPS, AFM and SEM characterization. This preservation translates into improved transistor performance, including enhanced ON currents, lower subthreshold slopes, narrower threshold voltage distributions, and a reduced device-to-device variability. Despite these advancements, PMMA residues still remain a significant challenge, impacting the cleanliness of the transferred layers and the overall reliability of 2D-TMDC-based devices. Future efforts should focus on identifying alternative polymers with high solubility to achieve cleaner interfaces while maintaining sufficient mechanical stiffness to prevent 2D-TMDC damage during transfer.

4. EXPERIMENTAL SECTION

MOCVD of 2D-WSe₂: The 2D-WSe₂ layer was epitaxially grown on sapphire (0001) using a commercial AIXTRON Close-Coupled Showerhead (CCS) reactor in 7×2" configuration. The sapphire was first desorbed at 1050°C in a 150 hPa H₂ atmosphere. Tungsten hexacarbonyl (W(CO)₆) and di-*iso*-propyl selenide (DiPSe) were used as tungsten and selenium precursors,

respectively, with H₂ as the carrier gas at 20 *hPa* reactor pressure. The growth temperature was 720°C, and the flow rates of W and Se precursors were 25 nm/min and 110 μmol/min, respectively.

Raman and photoluminescence spectroscopy: Non-resonant Raman measurements were performed at room temperature using a WiTec confocal microscope with a solid-state 532 nm laser. The laser line was focused on the sample by a 100× microscope objective lens. The collected light was dispersed by a grating with 1800 grooves/mm. The laser power was set to 1 *mW* to ensure a high signal-to-noise ratio and prevent laser-induced heating. The PL data was acquired with the same system using a 300 grooves/mm grating.

X-ray photoemission spectroscopy: For the XPS measurements, an AXIS Supra instrument (Kratos Analytical Ltd.) was used. Monochromatic X-rays are generated by an *Al Kα* source with an excitation energy of 1,486.6 eV. During data acquisition, charge neutralization with an electron-only source was performed to compensate for any charging effect. The high-resolution spectra were acquired with pass energy 10 eV and a step size of 0.05 eV. For quantitative analyses, the spectra were acquired with 20 eV pass energy and 0.1 eV step size. The binding energies were calibrated with respect to the *C1s* core level of hydrocarbons associated to adventitious carbon located at 284.8 eV.⁴⁹ For XPS core level analyses, a Shirley function for background subtraction followed by Voigt lineshape deconvolution was used.^{39,50}

Dry transfer of 2D-TMDC layers: In dry transfer, 950 *PMMA A6*, obtained from *Kayaku Advanced Materials, Inc*, was spin-coated at 3,000 *rpm* for 60 *s* on an as-grown 2D-TMDC/sapphire sample, and baked on a hot plate at 120 °C for 10 *min* in air (Figure 1c (ii)). As for the peel-off, the TRT applied was supplied by Nitto Revalpha (*no. P/N 319Y-4LS*) with an adhesion force of 4.8 N/20 mm on polyethylene terephthalate (PET). The PMMA plasma treatment (Fig. 1 (ix)) was performed in an ICP chamber (*SENTECH SI 500*) with a BCl₃/Ar plasma for

1 min, using gas flows of 10 and 20 standard cubic centimeters per minutes (*sccm*), for BCl_3 and Ar, respectively (ICP and RF power: 30 W).

Device fabrication: For the fabrication of globally back-gated 2D-WSe₂ field-effect transistors, after transferring (either wet or dry) the 2D layers onto p-type Si with 100 nm of thermally grown SiO₂ and removing the PMMA, metal contacts were defined by photolithography, metal deposition (Au, 80 nm), and lift-off processes. To define the device region, a photoresist layer was patterned by photolithography. Then, BCl_3 plasma (ICP and RF power: 30 W, 20 *sccm* BCl_3 + 10 *sccm* Ar) was used to etch away the unprotected 2D-TMDC layer before the photoresist layer was removed. More details of the device fabrication protocol are explained elsewhere.²⁵

ASSOCIATED CONTENT

Supporting Information

Detailed description of the in-depth XPS analysis of 2D layers and the dry transfer onto prepatterned substrate are provided in the supporting information.

AUTHOR INFORMATION

Corresponding Author

Amir Ghiami – *Compound Semiconductor Technology, RWTH Aachen University, 52074 Aachen, Germany*

Author Contributions

A.G. conceived the project and designed the experiments. A.G. carried out experiments and data analysis. H.F. helped with the SEM measurement and prepatterned substrate fabrication. T.S. helped with the electrical measurements. S.T., Y.W. and H.K. helped with the 2D-MoS₂ and 2D-WSe₂ MOCVD. E.M. and J.S. helped with the XPS measurement. A.P. helped with the wet

transfer. A.V., M.H. and M.C.L. did the funding acquisition. A.V. and H.K. supervised the project. A.G. wrote the manuscript. All authors discussed the results and commented on the manuscript.

Notes

The authors declare no competing financial interests

ACKNOWLEDGEMENT

This work has been financially supported by German Federal Ministry of Education and Research (BMBF), in the scope of NEUROTEC II (no. 16ME0399) and NeuroSys (no. 03ZU1106AA) projects.

REFERENCES

- (1) Qiu, H. *et al.* Two-Dimensional Materials for Future Information Technology: Status and Prospects. *Sci. China Inf. Sci.* **2024**, *67* (6), 160400. <https://doi.org/10.1007/s11432-024-4033-8>.
- (2) Lemme, M. C.; Akinwande, D.; Huyghebaert, C.; Stampfer, C. 2D Materials for Future Heterogeneous Electronics. *Nat. Commun.* **2021**, *13* (1), 1392. <https://doi.org/10.1038/s41467-022-29001-4>.
- (3) Lanza, M.; Radu, I. Electronic Circuits Made of 2D Materials. *Adv. Mater.* **2022**, *34* (48), 4–7. <https://doi.org/10.1002/adma.202207843>.
- (4) Zhu, J.; Park, J.-H.; Vitale, S. A.; Ge, W.; Jung, G. S.; Wang, J.; Mohamed, M.; Zhang, T.; Ashok, M.; Xue, M.; Zheng, X.; Wang, Z.; Hansryd, J.; Chandrakasan, A. P.; Kong, J.; Palacios, T. Low-Thermal-Budget Synthesis of Monolayer Molybdenum Disulfide for Silicon Back-End-of-Line Integration on a 200 Mm Platform. *Nat. Nanotechnol.* **2023**, *18* (5), 456–463. <https://doi.org/10.1038/s41565-023-01375-6>.
- (5) Zhang, Z.; Yang, X.; Liu, K.; Wang, R. Epitaxy of 2D Materials toward Single Crystals.

- Adv. Sci.* **2022**, *9* (8), 1–18. <https://doi.org/10.1002/advs.202105201>.
- (6) Tang, S.; Grundmann, A.; Fiadziushkin, H.; Ghiami, A.; Heuken, M.; Vescan, A.; Kalisch, H. Detailed Study on MOCVD of Wafer-Scale MoS₂ Monolayers: From Nucleation to Coalescence. *MRS Adv.* **2022**, *7* (30), 751–756. <https://doi.org/10.1557/s43580-022-00312-4>.
- (7) Tang, S.; Grundmann, A.; Fiadziushkin, H.; Wang, Z.; Hoffmann-Eifert, S.; Ghiami, A.; Debal, A.; Heuken, M.; Vescan, A.; Kalisch, H. Migration-Enhanced Metal–Organic Chemical Vapor Deposition of Wafer-Scale Fully Coalesced WS₂ and WSe₂ Monolayers. *Cryst. Growth Des.* **2023**, *23* (3), 1547–1558. <https://doi.org/10.1021/acs.cgd.2c01134>.
- (8) Grundmann, A.; Beckmann, Y.; Ghiami, A.; Bui, M.; Kardynal, B.; Patterer, L.; Schneider, J.; Kümmell, T.; Bacher, G.; Heuken, M.; Kalisch, H.; Vescan, A. Impact of Synthesis Temperature and Precursor Ratio on the Crystal Quality of MOCVD WSe₂ Monolayers. *Nanotechnology* **2023**, *34* (20), 205602. <https://doi.org/10.1088/1361-6528/acb947>.
- (9) Tang, H.; Pasko, S.; Krotkus, S.; Anders, T.; Wockel, C.; Mischke, J.; Wang, X.; Conran, B.; McAleese, C.; Teo, K.; Banerjee, S.; Silva, H. M.; Morin, P.; Asselberghs, I.; Ghiami, A.; Grundmann, A.; Tang, S.; Fiadziushkin, H.; Kalisch, H.; Vescan, A.; El Kazzi, S.; Marty, A.; Dosenovic, D.; Okuno, H.; Le Van-Jodin, L.; Heuken, M. Nucleation and Coalescence of Tungsten Disulfide Layers Grown by Metalorganic Chemical Vapor Deposition. *J. Cryst. Growth* **2023**, *608* (January), 127111. <https://doi.org/10.1016/j.jcrysgro.2023.127111>.
- (10) Kim, J.; Ju, X.; Ang, K.-W.; Chi, D. Van Der Waals Layer Transfer of 2D Materials for Monolithic 3D Electronic System Integration: Review and Outlook. *ACS Nano* **2023**, *17* (3), 1831–1844. <https://doi.org/10.1021/acsnano.2c10737>.

- (11) Watson, A. J.; Lu, W.; Guimarães, M. H. D.; Stöhr, M. Transfer of Large-Scale Two-Dimensional Semiconductors: Challenges and Developments. *2D Mater.* **2021**, *8* (3), 032001. <https://doi.org/10.1088/2053-1583/abf234>.
- (12) Nakatani, M.; Fukamachi, S.; Solís-Fernández, P.; Honda, S.; Kawahara, K.; Tsuji, Y.; Sumiya, Y.; Kuroki, M.; Li, K.; Liu, Q.; Lin, Y.-C.; Uchida, A.; Oyama, S.; Ji, H. G.; Okada, K.; Suenaga, K.; Kawano, Y.; Yoshizawa, K.; Yasui, A.; Ago, H. Ready-to-Transfer Two-Dimensional Materials Using Tunable Adhesive Force Tapes. *Nat. Electron.* **2024**, *7* (2), 119–130. <https://doi.org/10.1038/s41928-024-01121-3>.
- (13) Gurarslan, A.; Yu, Y.; Su, L.; Yu, Y.; Suarez, F.; Yao, S.; Zhu, Y.; Ozturk, M.; Zhang, Y.; Cao, L. Surface-Energy-Assisted Perfect Transfer of Centimeter-Scale Monolayer and Few-Layer MoS₂ Films onto Arbitrary Substrates. *ACS Nano* **2014**, *8* (11), 11522–11528. <https://doi.org/10.1021/nn5057673>.
- (14) Zhao, Y.; Song, Y.; Hu, Z.; Wang, W.; Chang, Z.; Zhang, Y.; Lu, Q.; Wu, H.; Liao, J.; Zou, W.; Gao, X.; Jia, K.; Zhuo, L.; Hu, J.; Xie, Q.; Zhang, R.; Wang, X.; Sun, L.; Li, F.; Zheng, L.; Wang, M.; Yang, J.; Mao, B.; Fang, T.; Wang, F.; Zhong, H.; Liu, W.; Yan, R.; Yin, J.; Zhang, Y.; Wei, Y.; Peng, H.; Lin, L.; Liu, Z. Large-Area Transfer of Two-Dimensional Materials Free of Cracks, Contamination and Wrinkles via Controllable Conformal Contact. *Nat. Commun.* **2022**, *13* (1), 4409. <https://doi.org/10.1038/s41467-022-31887-z>.
- (15) Sharma, M.; Singh, A.; Aggarwal, P.; Singh, R. Large-Area Transfer of 2D TMDCs Assisted by a Water-Soluble Layer for Potential Device Applications. *ACS Omega* **2022**, *7* (14), 11731–11741. <https://doi.org/10.1021/acsomega.1c06855>.
- (16) Kang, K.; Lee, K.-H.; Han, Y.; Gao, H.; Xie, S.; Muller, D. A.; Park, J. Layer-by-Layer Assembly of Two-Dimensional Materials into Wafer-Scale Heterostructures. *Nature* **2017**,

- 550 (7675), 229–233. <https://doi.org/10.1038/nature23905>.
- (17) Singh, A. P.; Xu, H.; Ghiami, A.; Tang, S.; Wang, Z.; Kalisch, H.; Hoffmann-Eifert, S.; Daus, A.; Ingebrandt, S.; Vescan, A.; Pachauri, V. Unravelling Chemical Etchant Influences during Assisted Wet-Transfer to Obtain High Quality MoS₂ Atomic Layers. *Appl. Surf. Sci.* **2024**, *669*, 160331. <https://doi.org/10.1016/j.apsusc.2024.160331>.
- (18) Kim, S.; Shin, S.; Kim, T.; Du, H.; Song, M.; Lee, C.; Kim, K.; Cho, S.; Seo, D. H.; Seo, S. Robust Graphene Wet Transfer Process through Low Molecular Weight Polymethylmethacrylate. *Carbon N. Y.* **2016**, *98*, 352–357. <https://doi.org/10.1016/j.carbon.2015.11.027>.
- (19) Liao, C.-D.; Capasso, A.; Queirós, T.; Domingues, T.; Cerqueira, F.; Nicoara, N.; Borme, J.; Freitas, P.; Alpuim, P. Optimizing PMMA Solutions to Suppress Contamination in the Transfer of CVD Graphene for Batch Production. *Beilstein J. Nanotechnol.* **2022**, *13*, 796–806. <https://doi.org/10.3762/bjnano.13.70>.
- (20) Kwon, J.; Seol, M.; Yoo, J.; Ryu, H.; Ko, D.-S.; Lee, M.-H.; Lee, E. K.; Yoo, M. S.; Lee, G.-H.; Shin, H.-J.; Kim, J.; Byun, K.-E. 200-Mm-Wafer-Scale Integration of Polycrystalline Molybdenum Disulfide Transistors. *Nat. Electron.* **2024**, *7* (5), 356–364. <https://doi.org/10.1038/s41928-024-01158-4>.
- (21) Yoon, T.; Shin, W. C.; Kim, T. Y.; Mun, J. H.; Kim, T.-S.; Cho, B. J. Direct Measurement of Adhesion Energy of Monolayer Graphene As-Grown on Copper and Its Application to Renewable Transfer Process. *Nano Lett.* **2012**, *12* (3), 1448–1452. <https://doi.org/10.1021/nl204123h>.
- (22) Huyghebaert, C.; Schram, T.; Smets, Q.; Kumar Agarwal, T.; Verreck, D.; Brems, S.; Phommahaxay, A.; Chiappe, D.; El Kazzi, S.; Lockhart De La Rosa, C.; Arutchelvan, G.;

- Cott, D.; Ludwig, J.; Gaur, A.; Sutar, S.; Leonhardt, A.; Marinov, D.; Lin, D.; Caymax, M.; Asselberghs, I.; Pourtois, G.; Radu, I. P. 2D Materials: Roadmap to CMOS Integration. *Tech. Dig. - Int. Electron Devices Meet. IEDM* **2019**, 2018-Decem, 22.1.1-22.1.4. <https://doi.org/10.1109/IEDM.2018.8614679>.
- (23) Velický, M.; Donnelly, G. E.; Hendren, W. R.; McFarland, S.; Scullion, D.; DeBenedetti, W. J. I.; Correa, G. C.; Han, Y.; Wain, A. J.; Hines, M. A.; Muller, D. A.; Novoselov, K. S.; Abruña, H. D.; Bowman, R. M.; Santos, E. J. G.; Huang, F. Mechanism of Gold-Assisted Exfoliation of Centimeter-Sized Transition-Metal Dichalcogenide Monolayers. *ACS Nano* **2018**, 12 (10), 10463–10472. <https://doi.org/10.1021/acsnano.8b06101>.
- (24) Li, M.-Y.; Hsu, C.-H.; Shen, S.-W.; Chou, A.-S.; Lin, Y. C.; Chuu, C.-P.; Yang, N.; Chou, S.-A.; Huang, L.-Y.; Cheng, C.-C.; Woon, W.-Y.; Liao, S.; Wu, C.-I.; Li, L.-J.; Radu, I.; Wong, H.-S. P.; Wang, H. Wafer-Scale Bi-Assisted Semi-Auto Dry Transfer and Fabrication of High-Performance Monolayer CVD WS₂ Transistor. In *2022 IEEE Symposium on VLSI Technology and Circuits (VLSI Technology and Circuits)*; IEEE, 2022; Vol. 2022-June, pp 290–291. <https://doi.org/10.1109/VLSITechnologyandCir46769.2022.9830376>.
- (25) Ghiami, A.; Sun, T.; Fiadziushkin, H.; Tang, S.; Grundmann, A.; Heuken, M.; Kalisch, H.; Vescan, A. Optimization of Layer Transfer and Photolithography for Device Integration of 2D-TMDC. *Crystals* **2023**, 13 (10), 1474. <https://doi.org/10.3390/cryst13101474>.
- (26) Sih, G. C. A Special Theory of Crack Propagation. In *Mechanics of Fracture Initiation and Propagation*; Springer Netherlands: Dordrecht, 1991; pp 1–22. https://doi.org/10.1007/978-94-011-3734-8_1.
- (27) Moriceau, H.; Rieutord, F.; Fournel, F.; Le Tiec, Y.; Di Cioccio, L.; Morales, C.; Charvet,

- A. M.; Deguet, C. Overview of Recent Direct Wafer Bonding Advances and Applications. *Adv. Nat. Sci. Nanosci. Nanotechnol.* **2011**, *1* (4), 043004. <https://doi.org/10.1088/2043-6262/1/4/043004>.
- (28) Plöbßl, A. Wafer Direct Bonding: Tailoring Adhesion between Brittle Materials. *Mater. Sci. Eng. R Reports* **1999**, *25* (1–2), 1–88. [https://doi.org/10.1016/S0927-796X\(98\)00017-5](https://doi.org/10.1016/S0927-796X(98)00017-5).
- (29) Evchuk, I. Y.; Musii, R. I.; Makitra, R. G.; Pristanskii, R. E. Solubility of Polymethyl Methacrylate in Organic Solvents. *Russ. J. Appl. Chem.* **2005**, *78* (10), 1576–1580. <https://doi.org/10.1007/s11167-005-0564-9>.
- (30) IRIYAMA, Y.; AMEMIYA, K.; IHARA, T. Effect of Plasma on the Degradation of Synthetic Polymers. *J. Photopolym. Sci. Technol.* **1995**, *8* (3), 403–410. <https://doi.org/10.2494/photopolymer.8.403>.
- (31) Ahmed, Q. S.; Bashir, S.; Jalil, S. A.; Shabbir, M. K.; Mahmood, K.; Akram, M.; Khalid, A.; Yaseen, N.; Arshad, A. Surface, Electrical and Mechanical Modifications of PMMA after Implantation with Laser Produced Iron Plasma Ions. *Nucl. Instruments Methods Phys. Res. Sect. B Beam Interact. with Mater. Atoms* **2016**, *378*, 1–7. <https://doi.org/10.1016/j.nimb.2016.04.035>.
- (32) Sakurabayashi, Y.; Masaki, T.; Iwao, T.; Yumoto, M. Surface Hardness Improvement of PMMA by Low-energy Ion Irradiation and Electron Irradiation. *Electron. Commun. Japan* **2011**, *94* (8), 19–26. <https://doi.org/10.1002/ecj.10350>.
- (33) Ton-That, C.; Shard, A. G.; Teare, D. O. H.; Bradley, R. H. XPS and AFM Surface Studies of Solvent-Cast PS/PMMA Blends. *Polymer (Guildf)*. **2001**, *42* (3), 1121–1129. [https://doi.org/10.1016/S0032-3861\(00\)00448-1](https://doi.org/10.1016/S0032-3861(00)00448-1).
- (34) Louette, P.; Bodino, F.; Pireaux, J.-J. Poly(Methyl Methacrylate) (PMMA) XPS Reference

- Core Level and Energy Loss Spectra. *Surf. Sci. Spectra* **2005**, *12* (1), 69–73.
<https://doi.org/10.1116/11.20050914>.
- (35) Bagiatis, V.; Critchlow, G. W.; Price, D.; Wang, S. The Effect of Atmospheric Pressure Plasma Treatment (APPT) on the Adhesive Bonding of Poly(Methyl Methacrylate) (PMMA)-to-Glass Using a Polydimethylsiloxane (PDMS)-Based Adhesive. *Int. J. Adhes. Adhes.* **2019**, *95* (June), 102405. <https://doi.org/10.1016/j.ijadhadh.2019.102405>.
- (36) Collaud, M.; Groening, P.; Nowak, S.; Schlapbach, L. Plasma Treatment of Polymers: The Effect of the Plasma Parameters on the Chemical, Physical, and Morphological States of the Polymer Surface and on the Metal-Polymer Interface. *J. Adhes. Sci. Technol.* **1994**, *8* (10), 1115–1127. <https://doi.org/10.1163/156856194X00979>.
- (37) Sui, S.; Li, L.; Shen, J.; Ni, G.; Xie, H.; Lin, Q.; Zhao, Y.; Guo, J.; Duan, W. Plasma Treatment of Polymethyl Methacrylate to Improve Surface Hydrophilicity and Antifouling Performance. *Polym. Eng. Sci.* **2021**, *61* (2), 506–513. <https://doi.org/10.1002/pen.25595>.
- (38) Schneider, D. S.; Grundmann, A.; Bablich, A.; Passi, V.; Kataria, S.; Kalisch, H.; Heuken, M.; Vescan, A.; Neumaier, D.; Lemme, M. C. Highly Responsive Flexible Photodetectors Based on MOVPE Grown Uniform Few-Layer MoS₂. *ACS Photonics* **2020**, *7* (6), 1388–1395. <https://doi.org/10.1021/acsp Photonics.0c00361>.
- (39) Ghiami, A.; Grundmann, A.; Tang, S.; Fiadziushkin, H.; Wang, Z.; Aussen, S.; Hoffmann-Eifert, S.; Heuken, M.; Kalisch, H.; Vescan, A. Impact of Carbon Impurities on Air Stability of MOCVD 2D-MoS₂. *Surfaces* **2023**, *6* (4), 351–363. <https://doi.org/10.3390/surfaces6040025>.
- (40) Jia, Y.; Gong, X.; Peng, P.; Wang, Z.; Tian, Z.; Ren, L.; Fu, Y.; Zhang, H. Toward High Carrier Mobility and Low Contact Resistance: Laser Cleaning of PMMA Residues on

- Graphene Surfaces. *Nano-Micro Lett.* **2016**, *8* (4), 336–346.
<https://doi.org/10.1007/s40820-016-0093-5>.
- (41) Choi, W.; Shehzad, M. A.; Park, S.; Seo, Y. Influence of Removing PMMA Residues on Surface of CVD Graphene Using a Contact-Mode Atomic Force Microscope. *RSC Adv.* **2017**, *7* (12), 6943–6949. <https://doi.org/10.1039/C6RA27436F>.
- (42) Liu, K. K.; Zhang, W.; Lee, Y. H.; Lin, Y. C.; Chang, M. T.; Su, C. Y.; Chang, C. S.; Li, H.; Shi, Y.; Zhang, H.; Lai, C. S.; Li, L. J. Growth of Large-Area and Highly Crystalline MoS₂ thin Layers on Insulating Substrates. *Nano Lett.* **2012**, *12* (3), 1538–1544. <https://doi.org/10.1021/nl2043612>.
- (43) Shi, W.; Lin, M.-L.; Tan, Q.-H.; Qiao, X.-F.; Zhang, J.; Tan, P.-H. Raman and Photoluminescence Spectra of Two-Dimensional Nanocrystallites of Monolayer WS₂ and WSe₂. *2D Mater.* **2016**, *3* (2), 025016. <https://doi.org/10.1088/2053-1583/3/2/025016>.
- (44) Liang, J.; Xu, K.; Toncini, B.; Bersch, B.; Jariwala, B.; Lin, Y.; Robinson, J.; Fullerton-Shirey, S. K. Impact of Post-Lithography Polymer Residue on the Electrical Characteristics of MoS₂ and WSe₂ Field Effect Transistors. *Adv. Mater. Interfaces* **2019**, *6* (3). <https://doi.org/10.1002/admi.201801321>.
- (45) Jayachandran, D.; Pendurthi, R.; Sadaf, M. U. K.; Sakib, N. U.; Pannone, A.; Chen, C.; Han, Y.; Trainor, N.; Kumari, S.; Mc Knight, T. V.; Redwing, J. M.; Yang, Y.; Das, S. Three-Dimensional Integration of Two-Dimensional Field-Effect Transistors. *Nature* **2024**, *625* (7994), 276–281. <https://doi.org/10.1038/s41586-023-06860-5>.
- (46) Cheng, Z.; Pang, C.-S.; Wang, P.; Le, S. T.; Wu, Y.; Shahrjerdi, D.; Radu, I.; Lemme, M. C.; Peng, L.-M.; Duan, X.; Chen, Z.; Appenzeller, J.; Koester, S. J.; Pop, E.; Franklin, A. D.; Richter, C. A. How to Report and Benchmark Emerging Field-Effect Transistors. *Nat.*

- Electron.* **2022**, 5 (7), 416–423. <https://doi.org/10.1038/s41928-022-00798-8>.
- (47) Mitta, S. B.; Choi, M. S.; Nipane, A.; Ali, F.; Kim, C.; Teherani, J. T.; Hone, J.; Yoo, W. J. Electrical Characterization of 2D Materials-Based Field-Effect Transistors. *2D Mater.* **2021**, 8 (1), 012002. <https://doi.org/10.1088/2053-1583/abc187>.
- (48) Sebastian, A.; Pendurthi, R.; Choudhury, T. H.; Redwing, J. M.; Das, S. Benchmarking Monolayer MoS₂ and WS₂ Field-Effect Transistors. *Nat. Commun.* **2021**, 12 (1), 693. <https://doi.org/10.1038/s41467-020-20732-w>.
- (49) Fang, D.; He, F.; Xie, J.; Xue, L. Calibration of Binding Energy Positions with C1s for XPS Results. *J. Wuhan Univ. Technol. Sci. Ed.* **2020**, 35 (4), 711–718. <https://doi.org/10.1007/s11595-020-2312-7>.
- (50) Ghiami, A.; Timpel, M.; Nardi, M. V.; Chiappini, A.; Nozar, P.; Quaranta, A.; Verucchi, R. Unravelling Work Function Contributions and Their Engineering in 2H-MoS₂ Single Crystal Discovered by Molecular Probe Interaction. *J. Phys. Chem. C* **2020**, 124 (12), 6732–6740. <https://doi.org/10.1021/acs.jpcc.0c00733>.

Supporting Information

Dry Transfer Based on PMMA and Thermal release Tape for Heterogeneous Integration of 2D-TMDC Layers

Amir Ghiami,^{†,} Hleb Fiadziushkin,[†] Tianyishan Sun,[†] Songyao Tang,[†] Yibing Wang,[†] Eva Mayer,[‡]
Jochen M. Schneider,[‡] Agata Piacentini,^{§,α} Max C. Lemme,^{§,α} Michael Heuken,^{†,§} Holger Kalisch,[†]
Andrei Vescan[†]*

[†] Compound Semiconductor Technology, RWTH Aachen University, 52074 Aachen, Germany

[‡] Materials Chemistry, RWTH Aachen University, 52074 Aachen, Germany

[§] Advanced Microelectronic Center Aachen (AMICA), AMO GmbH, Aachen, Germany

^α Chair of Electronic Devices, RWTH Aachen University, 52074 Aachen, Germany

[§] AIXTRON SE, 52134 Herzogenrath, Germany

* Email: ghiami@cst-rwth-aachen.de

Transfer onto prepatterned substrate

To further demonstrate the efficacy of the developed transfer process, an MOCVD 2D-MoS₂ layer was successfully transferred onto a prepatterned Si-SiO₂ substrate with Au metal contacts of 50 nm height (see Figure S1). This can be utilized for the fabrication of bottom-contact FET¹ and memristors².

Figure S1 shows the prepatterned substrate before and after the 2D-MoS₂ transfer and PMMA removal, achieving a near-perfect transfer success rate, with no visible pinhole or defects under optical microscope. This demonstrates that our dry transfer method can be successfully applied not only to Si-SiO₂ substrates but also to prepatterned Si-SiO₂ substrate with metal contacts, without adhering to the 30 nm limit mentioned by Kwon *et al.*³

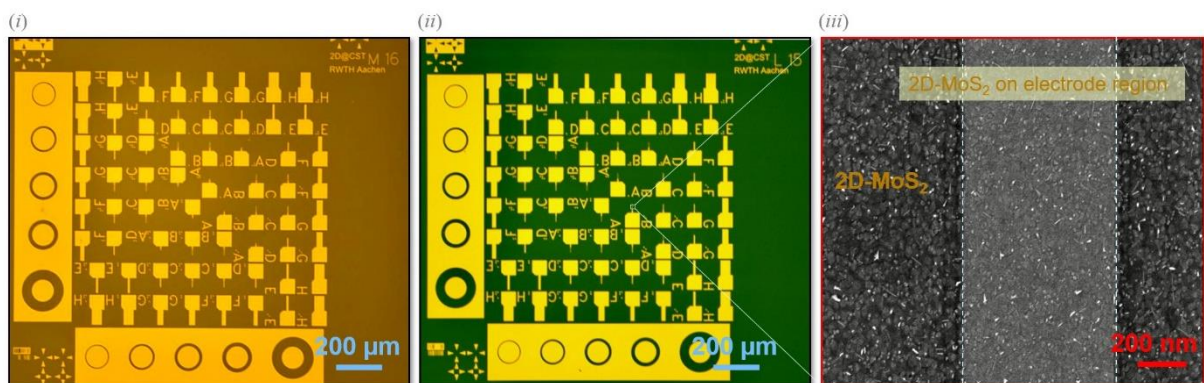


Figure S1. Dry transfer of the 2D-MoS₂ film onto the prepatterned substrate. (i) optical image of back electrodes fabricated on Si-SiO₂ substrate via photolithography and lift-off process, (ii) optical image of 2D-MoS₂ dry-transferred onto the prepatterned substrate (after PMMA removal), (iii) SEM image of the tip of an electrode with 2D-MoS₂ laying on top of it.

XPS analyses of 2D-TMDC layers

XPS analyses of as-deposited, wet-, and dry-transferred (after PMMA removal) 2D-MoS₂ and 2D-WSe₂ were performed. High resolution Mo3*d* and S2*p* core levels for 2D-MoS₂, and W4*f* and Se3*d* core levels for 2D-WSe₂ are shown in Figure S2 (i)-(iv). For 2D-MoS₂, the Mo3*d*_{5/2}, Mo3*d*_{3/2} and S2*s* peaks are located at 229.2 eV, 232.4 eV and 226.3 eV, while the S2*p*_{3/2} and S2*p*_{1/2} peaks are located at 162.0 eV and 163.2 eV, respectively, in good agreement with the values reported in literature.^{4,5}

The lineshapes verify the presence of pure MoS₂ in all as-deposited and transferred layers with neither oxide nor carbide species, which would have appeared at higher and lower binding energies relative to MoS₂ peaks, respectively. For 2D-WSe₂, W4*f*_{7/2}, W4*f*_{5/2} and W5*p*_{3/2} peaks are located at 32.6 eV, 34.9 eV and 38.3 eV, and the Se3*d*_{5/2} and Se3*d*_{3/2} peaks are located at 54.9 eV and 55.8 eV, respectively, also in good agreement with the values reported in literature.^{6,7} Similar to 2D-MoS₂, 2D-WSe₂ shows no oxidation peak, which would have appeared at higher binding energies relative to WSe₂ peaks. However, a peak located at lower binding energies relative to WSe₂ peaks can be detected, which is attributed to WSe_{2-x}C_x species likely co-deposited during

the MOCVD cool-down stage. This species is partially removed during the transfer, as suggested by its lower intensity in the transferred layers.

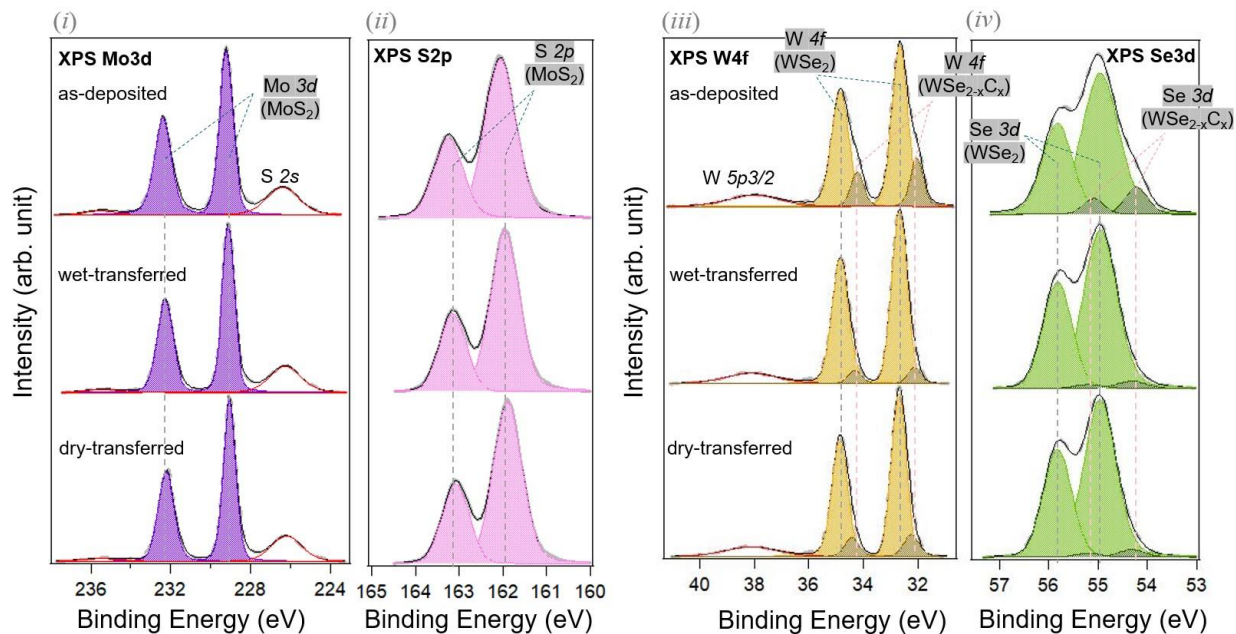


Figure S2. XPS analyses of as-deposited and transferred 2D-MoS₂ and 2D-WSe₂ layers. (i) Mo3d, (ii) S2p, and (iii) W4f, (iv) Se3d

References

- (1) Zhou, Y.; Tong, L.; Chen, Z.; Tao, L.; Pang, Y.; Xu, J.-B. Contact-Engineered Reconfigurable Two-Dimensional Schottky Junction Field-Effect Transistor with Low Leakage Currents. *Nat. Commun.* **2023**, *14* (1), 4270. <https://doi.org/10.1038/s41467-023-39705-w>.
- (2) Huh, W.; Lee, D.; Lee, C. Memristors Based on 2D Materials as an Artificial Synapse for Neuromorphic Electronics. *Adv. Mater.* **2020**, *32* (51), 1–16. <https://doi.org/10.1002/adma.202002092>.
- (3) Kwon, J.; Seol, M.; Yoo, J.; Ryu, H.; Ko, D.-S.; Lee, M.-H.; Lee, E. K.; Yoo, M. S.; Lee, G.-H.; Shin, H.-J.; Kim, J.; Byun, K.-E. 200-Mm-Wafer-Scale Integration of Polycrystalline

- Molybdenum Disulfide Transistors. *Nat. Electron.* **2024**, *7* (5), 356–364. <https://doi.org/10.1038/s41928-024-01158-4>.
- (4) Ganta, D.; Sinha, S.; Haasch, R. T. 2-D Material Molybdenum Disulfide Analyzed by XPS. *Surf. Sci. Spectra* **2014**, *21* (1), 19–27. <https://doi.org/10.1116/11.20140401>.
- (5) Ghiami, A.; Timpel, M.; Nardi, M. V.; Chiappini, A.; Nozar, P.; Quaranta, A.; Verucchi, R. Unravelling Work Function Contributions and Their Engineering in 2H-MoS₂ Single Crystal Discovered by Molecular Probe Interaction. *J. Phys. Chem. C* **2020**, *124*, 6732–6740. <https://doi.org/10.1021/acs.jpcc.0c00733>.
- (6) Shallenberger, J. R. 2D Tungsten Diselenide Analyzed by XPS. *Surf. Sci. Spectra* **2018**, *25* (1), 014001. <https://doi.org/10.1116/1.5016189>.
- (7) Grundmann, A.; Beckmann, Y.; Ghiami, A.; Bui, M.; Kardynal, B.; Patterer, L.; Schneider, J.; Kümmell, T.; Bacher, G.; Heuken, M.; Kalisch, H.; Vescan, A. Impact of Synthesis Temperature and Precursor Ratio on the Crystal Quality of MOCVD WSe₂ Monolayers. *Nanotechnology* **2023**, *34* (20), 205602. <https://doi.org/10.1088/1361-6528/acb947>.